HHS Public Access

Author manuscript

Oral Oncol. Author manuscript; available in PMC 2024 February 01.

Published in final edited form as:

Oral Oncol. 2023 February ; 137: 106304. doi:10.1016/j.oraloncology.2022.106304.

Intracellular Calprotectin (S100A8/A9) Facilitates DNA Damage Responses and Promotes Apoptosis in Head and Neck Squamous Cell Carcinoma

Prokopios P. Argyris[1,2,3,4,5,6,f], **Flávia Saavedra**[7], **Chris Malz**[7], **Ian A. Stone**[8], **Yuping Wei**[7], **William S. Boyle**[7], **Karen F. Johnstone**[7], **Ali Khammanivong**[2,9], **Mark C. Herzberg**[7,f]

[1]Department of Biochemistry, Molecular Biology and Biophysics, University of Minnesota, Minneapolis, MN, USA

[2]Masonic Cancer Center, University of Minnesota, Minneapolis, MN, USA

[3]Institute for Molecular Virology, University of Minnesota, Minneapolis, MN, USA

[4]Center for Genome Engineering, University of Minnesota, Minneapolis, MN, USA

[5]Howard Hughes Medical Institute, University of Minnesota, Minneapolis, MN, USA

[6]Division of Oral and Maxillofacial Pathology, School of Dentistry, University of Minnesota, Minneapolis, MN, USA

[7]Department of Diagnostic and Biological Sciences, School of Dentistry, University of Minnesota, Minneapolis, MN, USA

[8]Department of Immunology, Microbiology and Virology, School of Medicine and Dentistry, University of Rochester, Rochester, NY

[9]Department of Veterinary Clinical Sciences, College of Veterinary Medicine, University of Minnesota, St. Paul, MN, USA

Abstract

Objectives: In head and neck squamous cell carcinoma (HNSCC), poor prognosis and low survival are associated with downregulated calprotectin. Calprotectin (S100A8/A9) inhibits cancer cell migration and invasion and facilitates G2/M cell cycle arrest. We investigated whether S100A8/A9 regulates DNA damage responses (DDR) and apoptosis in HNSCC after chemoradiation.

Materials and Methods: Human HNSCC cases in TCGA were analyzed for relationships between S100A8/A9 and expression of apoptosis-related genes. Next, S100A8/A9-expressing and non-expressing carcinoma lines (two different lineages) were exposed to genotoxic agents and

[f]Correspondence to: argyr005@umn.edu and mcherzb@umn.edu.

The authors have no conflicts of interest to declare.

assessed for 53BP1 and γH2AX expression and percent of viable/dead cells. Finally, S100A8/A9-wild-type and S100A8/A9^{null} C57BL/6j mice were treated with 4-NQO to induce oral dysplastic and carcinomatous lesions, which were compared for endogenous levels of 53BP1.

Results: In S100A8/A9-high HNSCC tumors, apoptosis-related caspase family member genes were upregulated, whereas genes limiting apoptosis were significantly downregulated based on TCGA analyses. After X-irradiation or camptothecin treatment, S100A8/A9-expressing carcinoma cells (i.e., TR146 and KB-S100A8/A9) showed significantly higher 53BP1 and γH2AX recruitment, DNA fragmentation, proportions of dead cells, and greater sensitivity to cisplatin than wild-type KB or TR146-S100A8/A9-KD cells. Interestingly, KB-S100A8/A9$^{\Delta 113–114}$ cells showed similar 53BP1 and γH2AX levels to S100A8/A9-negative KB and KB-EGFP cells. After 4-NQO treatment, 53BP1 expression in oral lesions was significantly greater in calprotectin$^{+/+}$ than S100A8/A9^{null} mice.

Conclusions: In HNSCC cells, intracellular calprotectin is strongly suggested to potentiate DDR and promote apoptosis in response to genotoxic agents. Hence, patients with S100A8/A9-high HNSCC may encounter more favorable outcomes because more tumor cells enter apoptosis with increased sensitivity to chemoradiation therapy.

Keywords

S100A8/A9; calprotectin; head and neck squamous cell carcinoma; head and neck cancer; DNA damage; double-strand breaks; 53BP1; γH2AX; cisplatin; radiation

Introduction

Head and neck cancers, most frequently diagnosed as head/neck squamous cell carcinomas (HNSCC), represent the seventh most prevalent human malignancy worldwide accounting for 3% of all malignancies [1], and are associated with high morbidity and mortality [2, 3]. According to the American Cancer Society, 54,000 head/neck cancer cases are predicted to be diagnosed in 2022 in the United States, resulting in 11,230 deaths [4]. Notwithstanding advances in diagnosis and treatment, recurrent and/or metastatic disease develops in greater than 65% of patients with HNSCC [5]. Moreover, 5-year survival rates of HNSCC patients are only 50–60% [6–8].

HNSCCs are characterized by pronounced genomic instability; accumulated mutations drive neoplastic cells to initiate or facilitate carcinogenesis [9]. The development of HNSCC is strongly associated with exogenous mutagenic factors including tobacco metabolites and alcohol consumption [10, 11]. Independently of alcohol and tobacco exposure, high-risk human papillomavirus (HPV) infection (i.e., HPV16 and HPV18) is mechanistically linked to HNSCC through the E6 and E7 viral oncoproteins, which inactivate p53 and Rb, respectively [6, 12]. The high-risk HPV viruses also induce the APOBEC3 family of ssDNA cytosine deaminases [13–17], which cause a significant fraction of point mutations in HNSCC tumors [18–20].

Within cells, DNA damage responses (DDR) function to rectify DNA damage and circumvent lethal or permanent genetic alteration [21]. Coordinated by the ATM-Chk1/Chk2 phosphorylation signaling pathway, DDR activates DNA damage checkpoints. The activated

checkpoints arrest the cell cycle at G1/S or G2/M, which facilitates DNA repair [22]. Coincident with cell cycle arrest, DDR activation occurs by phosphorylation of DNA repair scaffold proteins H2AX, 53BP1, BRCA1 and SMC1 [23, 24]. Unrepaired or misrepaired DNA damage can activate programmed cell death (apoptosis) or senescence or promote carcinogenesis by increasing genomic instability [24, 25].

In HNSCC cells, calprotectin (S100A8/A9) functions as a tumor suppressor activating the G2/M DNA damage checkpoint to control cell cycle progression, proliferation, and growth [26, 27]. In contrast, loss of S100A8/A9 enhances MMP-2 activity, cell invasion, and migration [27, 28]. Calprotectin, a heterodimeric complex of S100A8 and S100A9, is constitutively expressed in the cytoplasm of the squamous epithelial cells lining the oral, oropharyngeal, and genitourinary mucosae [27, 29]. Whether the sole phosphorylatable residue in calprotectin, S100A9^{Thr113} [30] participates in tumor suppression is unknown. Members of the S100 superfamily of EF-hand calcium-binding proteins [31–33], *S100A8* and *S100A9* are located within the epidermal differentiation complex on chromosome 1q21, and their products appear to contribute to epithelial maturation and growth [34].

Consequently, reduced expression of calprotectin is expected to be associated with epithelial dedifferentiation. As predicted, calprotectin expression levels in HNSCC patients are inversely associated with tumor grade [35] and positively related to better survival outcomes [31]. Since cell cycle arrest at G2/M constitutes a hallmark of the DDR pathway, we *hypothesized* that S100A8/A9 regulates DNA repair events following exposure of HNSCC cells to genotoxic agents.

Materials and Methods

Stable knockdown of S100A8/A9 in a human HNSCC cell line

TR146 cells, a well-differentiated buccal SCC cell line, was silenced for endogenous S100A8/A9 expression (TR146-S100A8/A9-KD) using shRNA as described [26, 35, 36]. Cells transfected with a vector containing scrambled shRNA provided a negative control for S100A8 and S100A9 gene-silenced clones (TR146-control) as described [26, 36]. Calprotectin levels were confirmed using Western blotting.

Stable expression of S100A8/A9 in a human carcinoma cell line

KB cells (ATCC CCL-17), a HeLa-like, HPV-18-positive, calprotectin-negative, human carcinoma cell line, was utilized [32]. KB cells stably expressing wild-type human calprotectin (KB-S100A8/A9), a truncated non-phosphorylatable calprotectin clone (KB-S100A8/A9$^{\Delta 113–114}$), and KB sham-control transfectants (KB-EGFP) were generated and cultured as described [30]. Transfected cells were selected and maintained in G418 sulfate (Corning, #30–234-CR) in an appropriate cell culture medium [26, 36]. Cytosolic S100A8/A9 production was verified in cell lysates using Western blot analysis; S100A8/A9 release into culture medium was below the limits of detection by ELISA, mitigating the chance of extracellular interactions (data not shown).

Treatment with camptothecin and X-radiation to induce DNA damage

Camptothecin (Sigma, #C9911) was dissolved in chloroform/methanol (4:1) to 5 mg/mL. The solution was diluted into complete medium to a final concentration of 10 μM and used to treat cells growing at 70–80% confluence on glass coverslips for 4 h. DNA damage was induced by irradiation using the X-Rad 320 X-ray system (PXi Precision X-Ray, North Branford, CT). The source was placed 50 cm from the irradiator stage. A constant voltage potential of 320 kV was applied and the current was set at 12.5 mA. The radiation dose delivered to the cells/minute was adjusted using a copper and aluminum compound filter. In this study, a total dose of 100, 300, 500, or 700 cGy was delivered to each cell culture sample.

Cisplatin treatment and cell viability assay

TR146 and KB cell lines (2×10^5 in 100 μL) were seeded in triplicate for each cisplatin concentration (1, 10, 50 and 100 μM) in flat-bottom 96-well microtiter plates and incubated in 5% CO_2 at 37°C for 24 h. After 24 h of incubation, cell viability was analyzed using the XTT Cell Proliferation Assay Kit (ATCC, Cat# 30–1011K). Activated-XTT solution (50 μL) was added to each well, incubated for 2 more hours, and absorbance was measured at 450 nm and 675 nm using a microtiter plate reader. The 450 nm values were subtracted from the values obtained at 675 nm to eliminate potential non-specific readings.

Immunofluorescence microscopy to localize DNA damage markers 53BP1 and γH2AX

To localize 53BP1 and γH2AX in response to DNA damaging agents (i.e., camptothecin and X-radiation), cells growing on coverslips in 6-well plates were fixed in ice-cold methanol and permeabilized for 10 min with PBS containing 0.25% Triton X-100 (PBS-T). To block non-specific binding of primary antibodies, cells were incubated for 30 min in 1% BSA in PBS-T. Rabbit polyclonal anti(α)-53BP1 (Abcam, ab36823, 1:200 dil.) and mouse monoclonal α-γH2AX (phospho S139; 9F3, Abcam, ab26350, 1:200 dil.) antibodies were diluted in PBS-T containing 1% BSA, incubated with cells for 1 to 2 h in a humidified chamber, and washed 3X for 5 min each with PBS. Cells were then incubated in the dark for 60 min with Alexa Fluor 488-conjugated goat anti-rabbit IgG (H+L) (Thermo Fisher Scientific, #A32731) and Alexa Fluor 568-conjugated goat anti-mouse IgG (H+L) (Thermo Fisher Scientific, #A-11036) secondary antibodies diluted 1:500 in 1% BSA/PBS-T. Specimens were visualized using a Nikon Eclipse E800 upright fluorescence microscope. Images were captured via SPOT advance software (Spot Imaging, Sterling Heights, MI, USA) and subsequently analyzed using ImageJ. At least 100 cells were evaluated per cell line and condition in each experiment. Statistical analyses were performed using GraphPad Prism 8.

Comet assay

Each cell line was cultured separately in 6-well plates as described [26, 30, 36] and grown to 70–80% confluence. Double-strand breaks were induced by a single X-ray dose of 5 Gy. After 30 min, 2 h, and 24 h cells were harvested and resuspended in ice-cold 1X Dulbecco's-PBS (Ca^{2+} and Mg^{2+} free, 1×10^5 cells /mL). Double-strand breaks and DNA repair were assessed using single cell gel electrophoresis (comet assay) following the manufacturer's

protocol (Oxiselect™ Comet Assay Kit; #STA-351 Cell Biolabs, Inc., San Diego, CA). The cell suspension was mixed at a 1:10 ratio (v/v) with comet kit agarose, and 75 μL were immediately plated on Oxiselect™ comet slides at 4°C for 15 min, allowing the agarose-cell suspension to solidify. Cell electrophoresis was performed according to the manufacturer's alkaline comet assay protocol, which can resolve the double-strand breaks produced by the genotoxic agents used in our study. Specimens were visualized and photographed as above.

Post-irradiation SYTO 9/propidium iodide live/dead assay

After inducing DNA damage, the fraction of late apoptotic and/or necrotic cells was assessed at 30 min, 2 h and 24 h post-irradiation using a live/dead viability assay kit (LIVE/DEAD® *Bac*Light™ Kit; L7012, Invitrogen, Carlsbad, CA) according to the manufacturer's instructions. Growth medium was removed, and adherent cells were rinsed gently with 1 mL 1X Dulbecco's-PBS at room temperature. SYTO 9/propidium iodide fluorescence dyes were mixed according to the manufacturer's protocol. Cells were incubated in 3 μL of the dye mixture per mL of PBS in each well for 15 min in the dark. Next, the samples were mounted on glass slides using *Bac*Light mounting oil and visualized as above. Red-stained (propidium iodide) nuclei were considered apoptotic, while green-stained (SYTO 9) cells were viable. Data were analyzed as above.

53BP1 and S100A8 expression in 4-NQO-induced murine oral lesions

To induce oral carcinogenesis, 4-NQO (50 μg/ml *ad libitum*) was added to the water of C57BL/6j wild-type (N = 12) and S100A8/A9^{null} mice (N = 12) for 16 weeks as described [37, 38]. During weeks 17 to 22, animals received water without 4-NQO. Control mice (n=6 each genotype) received water without 4-NQO during the entire 22-week experiment. All animals were euthanized at 22 weeks. The tongue, maxillary gingiva, palate, and buccal mucosae were harvested for histopathologic examination using H/E staining. Intraoral epithelial dysplastic and/or carcinomatous lesions from 4-NQO-treated wild-type and S100A8/A9^{null} mice (N = 7 in each group) were immunostained for 53BP1 (Abcam, ab36823, 1:200 dil.) and S100A8 (R&D, AF3059, 1:500 dil.) as described [35]. Staining for S100A8 was used as a surrogate for S100A8/A9. At least 2 microscopic lesions per animal were selected and 20X-magnification photomicrographs per lesion were captured using the Leica DM6 B (Leica Microsystems CMS GmbH) microscope. Quantification of 53BP1 positive nuclei and statistical analysis were performed as above.

Results

Calprotectin expression is associated with elevated caspase transcription levels and facilitates apoptosis in HNSCC

As we have shown, calprotectin-expressing carcinoma cells have a less aggressive phenotype [26, 28], and patients with calprotectin-high HNSCC have more favorable survival outcomes compared to patients with calprotectin-low tumors [27, 31]. To determine whether calprotectin expression in HNSCC affects the expression of genes associated with apoptosis, cell death, and survival, we interrogated transcriptomic data from TCGA RNA sequencing database. In S100A8/A9-high HNSCCs, expression of 363 apoptosis-related genes was significantly upregulated compared to S100A8/A9-low neoplasms. Co-regulated with

S100A8 and *S100A9*, apoptosis-associated genes including the caspase family members *CASP1*, *-3, -4, -5, - 7, -8, -9, -10* and *-14* showed significant fold-increases in S100A8/A9-high relative to S100A8/A9-low HNSCC (range: 1.48- to 9.54-fold; Table 1). S100A8/A9-expressing human HNSCCs also upregulated genes that facilitate cell death (e.g., *XAF1*) based on TCGA analyses (Figure 1A). In addition, KB carcinoma cells engineered to express S100A8/A9 significantly downregulated *XIAP* (X-linked inhibitor of apoptosis) *in vitro* (Figure 1B), suggesting that calprotectin exerts pro-apoptotic functions in human HNSCC.

S100A8/A9 promotes DDR after treatment with camptothecin and X-irradiation

We treated calprotectin-positive and negative KB carcinoma cell lines with the DNA damage agent camptothecin (Figure 2A–C) and assessed the levels of the DNA damage regulatory proteins, 53BP1 and γH2AX. Following camptothecin treatment, calprotectin-expressing KB cells showed significantly greater percentages of 53BP1 (Figure 2A,B) and γH2AX (Figure 2A,C) positive nuclei than calprotectin-negative (KB wild-type, KB-EGFP) cells. Interestingly, the high number of 53BP1 (Figure 2B) and γH2AX (Figure 2C) nuclear puncta in calprotectin-expressing KB cells increased only slightly with camptothecin treatment. In response to camptothecin, expression of 53BP1 (Figure 2A,B) and γH2AX (Figure 2A,C) was similar in KB-S100A8/A9$^{\Delta 113–114}$ cells (missing the single phosphorylatable S100A9^{Thr113}) and calprotectin-negative KB and KB-EGFP carcinoma cells. These data suggest that the phosphorylation state of S100A9^{Thr113} in calprotectin is important in the regulation of 53BP1 and γH2AX recruitment during DDR.

For patients with HNSCC, X-irradiation is a primary treatment option along with surgery and chemotherapy. To further investigate the participation of S100A8/A9 in post-irradiation DDR, we exposed the KB cancer cell lines to increasing doses of X-irradiation (0 to 7 Gy; Figure 2D–F). In the absence of X-irradiation, 53BP1 (Figure 2D,E) and γH2AX levels (Figure 2D,F) were significantly higher in calprotectin-expressing KB cells than in calprotectin-negative cells. In the same conditions, KB-S100A8/A9$^{\Delta 113–114}$ cells showed about 20% fewer 53BP1 (Figure 2D,E) and γH2AX puncta (Figure 2D,F) than KB-S100A8/A9 cells. Irradiated calprotectin-expressing KB cells also showed greater 53BP1 (Figure 2E) and γH2AX (Figure 2F) nuclear recruitment at all doses of X-radiation than calprotectin-negative or KB-S100A8/A9$^{\Delta 113–114}$ cells, which were similar to one another. In all KB cell lines, the DDR protein levels increased most as X-irradiation doses increased from 0 to 1 Gy (Figure 2E,F).

Camptothecin treatment of TR146 buccal carcinoma cell lines confirmed DDR dependence on calprotectin expression (Figure 3). In untreated cells (no camptothecin), silencing calprotectin (TR146-S100A8/A9-KD; Figure 3A) caused significantly fewer 53BP1 (Figure 3B) and γH2AX (Figure 3C) positive nuclei than calprotectin-positive (TR146 and TR146-control) cells. After incubation with camptothecin, 53BP1 and γH2AX nuclear recruitment increased in all TR146 cell lines (Figure 3A). Calprotectin-expressing TR146 cells (TR146 and TR146-control), however, showed significantly higher percentages of 53BP1 (Figure 3B) and γH2AX (Figure 3C) puncta than cells with silenced calprotectin (TR146-S100A8/A9-KD).

Following all doses of X-irradiation, nuclear recruitment of 53BP1 (Figure 3D,E) and γH2AX (Figure 3D,F) was more significantly impaired in TR146-S100A8/A9-KD than in calprotectin-expressing TR146 and TR146-control cells. Both TR146 and TR146-control cell lines showed similarly elevated percentages of 53BP1 and γH2AX positive nuclei after X-irradiation (Figure 3D–F). Collectively, these *in vitro* data strongly suggest that calprotectin contributes to DDR in response to genotoxic agents.

Calprotectin promotes apoptotic DNA fragmentation following X-irradiation and cisplatin-induced cell death in HNSCC cells

Activation of apoptosis induces DNA fragmentation and is driven by members of the caspase family of enzymes [39, 40], many of which appear to be co-regulated with *S100A8* and *S100A9* (see Table 1). We *hypothesized*, therefore, that S100A8/A9 facilitates nuclear fragmentation in response to genotoxic X-irradiation. After 5 Gy X-irradiation, the length and frequency of nuclear fragmentation (i.e., comet tail formation) were compared in calprotectin-expressing TR146, TR146-S100A8/A9-KD, and control-transfected TR146 cells. For up to 24 h after exposure, S100A8/A9-producing TR146 and TR146-transfection-control cells appeared to be more sensitive to X-irradiation and showed greater nuclear fragmentation than in calprotectin silenced cells (Figure 4A). At 24 h after X-irradiation, calprotectin-expressing TR146 and TR146-transfection-control cultures showed significantly more dead cells (Figure 4B,C) and significantly less resistance to cisplatin treatment (Figure 4D) than TR146-S100A8/A9-KD cells.

These calprotectin-dependent responses were cell lineage-independent since calprotectin-overexpressing (KB-S100A8/A9) cells showed greater comet tail formation than calprotectin-negative KB and KB-EGFP cells (Figure 5A). Similarly, KB-S100A8/A9 cells showed significantly higher proportions of dead cells up to 24 h post-X-irradiation (Figure 5B,C) and significantly greater sensitivity to the DNA damage therapeutic, cisplatin, (Figure 5D) than calprotectin-negative KB and KB-EGFP cells.

Calprotectin-dependent DDR in carcinogen-induced mouse oral epithelial dysplastic and carcinomatous lesions

To learn whether DNA damaging agents cause a calprotectin-dependent difference in the DDR *in vivo*, C57BL/6j mice were challenged with 4-NQO in their drinking water for 16 weeks and evaluated for oral epithelial dysplastic and carcinomatous lesions at 22 weeks (Figure 6A). In the dysplastic lingual epithelium of calprotectin-expressing wild-type mice, 53BP1 puncta were prominent. These puncta were less apparent in frank SCC tumors, which were marked by the loss of the calprotectin-subunit S100A8 (Figure 6B). In contrast, calprotectin-negative mice rarely showed 53BP1 expression in tongue dysplastic and carcinomatous lesions (Figure 6C). Based on quantification of all lesions in all mice, 53BP1 expression was significantly greater in WT calprotectin-expressing mice than in the calprotectin-negative mutants (Figure 6D).

Discussion

Intracellular calprotectin is strongly suggested to have tumor suppressive properties in HNSCC based upon experiments utilizing oral carcinoma cell lines, human oral and oropharyngeal tumor specimens, animal models, and analysis of publicly available databases [26–28, 31, 35]. Key mechanistic evidence is provided *in vitro*. S100A8/A9 negatively regulates the G2/M cell cycle checkpoint and then slows cancer cell proliferation. Overexpression of cytoplasmic S100A8/A9 promotes increased protein phosphatase 2A (PP2A) activity, triggers phosphorylation of p-Chk1 (Ser345), and dephosphorylates p-Cdc25C at Thr48 by PP2A. This mechanism allows p-Chk1 to phosphorylate Cdc25C at the inhibitory residue, Ser216. Calprotectin status does not appear to affect the regulation of G1/S cell cycle checkpoint under control by p53 and p21 in carcinoma cells [26]. The cyclin B1/p-Cdc2 (Thr14/Tyr15) G2/M regulatory complex remains inactive, however, arresting cell cycle at G2/M (Supplementary Figure 1) [26].

Activation of the G2/M checkpoint and cell cycle arrest are connected to the DDR pathway, a cellular response to severe genotoxicity (Supplementary Figure 1) [21, 22, 41]. In head and neck cancers, DDR is activated by cellular exposure to exogenous (i.e., cisplatin-based chemotherapeutics and X-irradiation) and endogenous (i.e., APOBEC3-induced C-to-T/-G deamination) mutagens. The occurrence of DNA double-strand breaks [42] and the error-prone repair of DNA through non-homologous end joining signal the nuclear localization of 53BP1 puncta [43]. Functionally linked with 53BP1, γH2AX (Ser139) [42] serves as a scaffold for other repair proteins and contributes to nucleosome formation and chromatin remodeling [44].

To study the effect of intracellular calprotectin on genotoxicity in head/neck carcinoma cells, we used 53BP1 and γH2AX as DDR markers. DNA double-strand breaks and activation of apoptotic cell death were induced using X-irradiation [45]. In contrast, camptothecin, which acts by reversibly binding to DNA-topoisomerase I complexes to inhibit DNA unwinding, was also used to promote cell cycle arrest and apoptosis [46]. We discovered that DDR phenomena *in vitro* in response to these genotoxic stimuli were dependent on S100A8/A9 expression. Both treatments caused significantly increased accumulation of 53BP1 and γH2AX puncta in the nuclei of S100A8/A9-expressing cells. In contrast, S100A8/A9-negative carcinoma cells show dramatically impaired DDR responses with limited numbers of observed 53BP1- and γH2AX-positive nuclei. Since S100A8/A9 appears to restore the G2/M cell cycle checkpoint [26] and cell cycle arrest represents an early event in the DDR pathway, we anticipated a role for calprotectin in other DDR functions including recruitment of DNA repair-associated molecules.

To participate in DDR, the S100A8/A9 complex would likely translocate from the cytoplasm into the nucleus. Indeed, calprotectin apparently co-localizes with casein-kinase 2 on the mitotic spindles of dividing non-cancerous (immortalized TERT-2/OKF-6) and carcinomatous (TR146) cells (Argyris et al. manuscript in preparation). Nuclear-specific S100A8/A9 also controls oncogenic transcription and transformation in breast cancer [47]. Clinical specimens of breast and skin cancers [47] and HNSCC [35] also show clear S100A8 and S100A9 nuclear immunohistochemical staining. Collectively, our data strongly suggest

that S100A8/A9 activates the G2/M checkpoint and cell cycle arrest to regulate DDR, with subsequent recruitment of 53BP1 and γH2AX.

We also show that cytoplasmic calprotectin promotes DNA fragmentation and facilitates apoptosis in HNSCC cells after exposure to chemoradiation. Indeed, S100A8/A9 expression in HNSCC cells appears to confer sensitivity to both X-irradiation and cisplatin treatment and increases susceptibility to death by apoptosis. Conversely, calprotectin-negative carcinoma cells evade post-radiation DNA fragmentation and appear refractory to chemoradiation. After X-irradiation, caspase-3/7 activity is also significantly elevated in calprotectin-expressing HNSCC cells compared to S100A8/A9-negative cells as we reported [35]. These data highlight that calprotectin plays a regulatory role in chemoradiation-induced cell death. Imprecise repair of DNA damage activates programmed cell death. Evasion of apoptotic cellular mechanisms and sustained proliferative signaling are two well-established hallmarks of carcinogenesis [48].

A mechanistic link between calprotectin and apoptosis is supported by evidence from patient HNSCC tumors. Indeed, S100A8/A9-high HNSCCs significantly upregulate apoptosis-related genes, including *CASP-3, -4, -5, -7, -8,* and *-9,* when compared to S100A8/A9-low tumors as analyzed using TCGA data. As we show *in vitro*, cytoplasmic calprotectin in tumor cells potentiates 53BP1 and γH2AX nuclear recruitment, strongly favoring apoptotic cell death rather than DNA repair. Apoptosis-associated DNA fragmentation is also marked by γ-phosphorylation of H2AX (Ser139) [49], while a close association between 53BP1, γH2AX, and cleaved caspase-3 also appears linked to increased cell death in murine tissues [50, 51].

In addition to the effects of cytoplasmic and nuclear translocation, calprotectin release into the extracellular environment promotes autophagy and apoptosis *in vitro*. Purified recombinant S100A8 and S100A9 treatment of cell lines, including colon and prostate adenocarcinoma, cervical SCC, and acute promyelocytic leukemia, inhibits cancer cell migration and growth and promotes cell death [52–55]. The beneficial effects of calprotectin on DDR and apoptosis in clinical cases may reflect extracellular and intracellular modes of action.

Interestingly, the DDR responses to camptothecin and X-irradiation appear to be dependent on the phosphorylation state of S100A8/A9. Calprotectin has a singular phosphorylatable site at the penultimate $S100A9^{Thr113}$ residue in the C-terminus. When phosphorylated through Ca^{2+} and p38 MAPK signaling during inflammation, neutrophil microtubules reorganize to enable cell migration [56] and activation of NADPH oxidase [57], inducing proinflammatory TNFα and IL-6 expression and release [58]. As we show, Thr113 removal (KB-$S100A8/A9^{\Delta 113–114}$ cells) results in a DDR-insensitive phenotype, indistinguishable from calprotectin negative cells, as compared to S100A8/A9-expressing cells. Although the phosphorylation status of calprotectin was not directly assessed in the experiments of the current study, the dramatic change in DDR after S100A9 tail truncation by the two amino acids suggests that $S100A9^{Thr113}$ participates in a phosphorylation cascade (see Supplementary Figure 1). We speculate that ATM phosphorylates calprotectin at Thr113 like numerous other DDR-associated proteins including 53BP1, H2AX, and SMC1 [59].

In summary, we provide additional evidence in support of the anti-tumor properties of intracellular calprotectin in HNSCC. Expression of S100A8/A9 potentiates DDR, confers sensitivity to chemoradiation, and overtly promotes apoptotic cancer cell death. These findings may explain the more favorable survival outcomes reported in patients with S100A8/A9-high HNSCC than in individuals with S100A8/A9-low tumors [26]. These results provide a basis for future translational studies investigating the therapeutic potential of calprotectin to suppress tumors in HNSCC patients.

Supplementary Material

Refer to Web version on PubMed Central for supplementary material.

Acknowledgements

The project was supported by NIH/NIDCR R01DE021206 to MCH and R90DE023058 to PPA. The content is solely the responsibility of the authors and does not necessarily represent the official views of the NIDCR or the NIH. The authors thank Dr. Shorouk Elnagdy for assistance with the mice in the 4-NQO protocol, Drs. Rajaram Gopalakrishnan and Ioannis G. Koutlas, University of Minnesota, for assistance with mouse tissue processing for histopathologic analysis, and Dr. Gay Herzberg for expert editing.

References

[1]. Chow LQM. Head and Neck Cancer. N Engl J Med. 2020;382:60–72. [PubMed: 31893516]

[2]. Cai Y, Dodhia S, Su GH. Dysregulations in the PI3K pathway and targeted therapies for head and neck squamous cell carcinoma. Oncotarget. 2017;8:22203–17. [PubMed: 28108737]

[3]. Ferlay J, Shin HR, Bray F, Forman D, Mathers C, Parkin DM. Estimates of worldwide burden of cancer in 2008: GLOBOCAN 2008. Int J Cancer. 2010;127:2893–917. [PubMed: 21351269]

[4]. Society. AC. Key Statistics for Oral Cavity and Oropharyngeal Cancers. Available from: https://www.cancer.org/cancer/oral-cavity-and-oropharyngeal-cancer/about/key-statistics.html [Accessed 05/12/2022].

[5]. Argiris A, Karamouzis MV, Raben D, Ferris RL. Head and neck cancer. Lancet. 2008;371:1695–709. [PubMed: 18486742]

[6]. El-Naggar AKCJ, Grandis JR, Takata T, Ed. SP. Tumours of the oral cavity and mobile tongue. In: World Health Organization (WHO) Classification of Head and Neck Tumours: International Agency for Research on Cancer (IARC). 4th Edition. Lyon: pp 105–115; 2017.

[7]. Miller KD, Siegel RL, Lin CC, Mariotto AB, Kramer JL, Rowland JH, et al. Cancer treatment and survivorship statistics, 2016. CA Cancer J Clin. 2016;66:271–89. [PubMed: 27253694]

[8]. Warnakulasuriya S Global epidemiology of oral and oropharyngeal cancer. Oral Oncol. 2009;45:309–16. [PubMed: 18804401]

[9]. Hanahan D, Weinberg RA. The hallmarks of cancer. Cell. 2000;100:57–70. [PubMed: 10647931]

[10]. Sivasithamparam J, Visk CA, Cohen EE, King AC. Modifiable risk behaviors in patients with head and neck cancer. Cancer. 2013;119:2419–26. [PubMed: 23575663]

[11]. D'Souza G, Kreimer AR, Viscidi R, Pawlita M, Fakhry C, Koch WM, et al. Case-control study of human papillomavirus and oropharyngeal cancer. N Engl J Med. 2007;356:1944–56. [PubMed: 17494927]

[12]. Dok R, Nuyts S. HPV Positive Head and Neck Cancers: Molecular Pathogenesis and Evolving Treatment Strategies. Cancers (Basel). 2016;8:41. [PubMed: 27043631]

[13]. Vieira VC, Leonard B, White EA, Starrett GJ, Temiz NA, Lorenz LD, et al. Human papillomavirus E6 triggers upregulation of the antiviral and cancer genomic DNA deaminase APOBEC3B. MBio. 2014; 5:e02234–14. [PubMed: 25538195]

[14]. Mori S, Takeuchi T, Ishii Y, Kukimoto I. Identification of APOBEC3B promoter elements responsible for activation by human papillomavirus type 16 E6. Biochem Biophys Res Commun. 2015;460:555–60. [PubMed: 25800874]

[15]. Mori S, Takeuchi T, Ishii Y, Yugawa T, Kiyono T, Nishina H, et al. Human Papillomavirus 16 E6 upregulates APOBEC3B via the TEAD transcription factor. J Virol. 2017;91:e02413–16. [PubMed: 28077648]

[16]. Westrich JA, Warren CJ, Klausner MJ, Guo K, Liu CW, Santiago ML, et al. Human Papillomavirus 16 E7 Stabilizes APOBEC3A Protein by Inhibiting Cullin 2-Dependent Protein Degradation. J Virol. 2018;92:e01318–17. [PubMed: 29367246]

[17]. Warren CJ, Xu T, Guo K, Griffin LM, Westrich JA, Lee D, et al. APOBEC3A functions as a restriction factor of human papillomavirus. J Virol. 2015;89:688–702. [PubMed: 25355878]

[18]. Burns MB, Lackey L, Carpenter MA, Rathore A, Land AM, Leonard B, et al. APOBEC3B is an enzymatic source of mutation in breast cancer. Nature. 2013;494:366–70. [PubMed: 23389445]

[19]. Alexandrov LB, Kim J, Haradhvala NJ, Huang MN, Tian Ng AW, Wu Y, et al. The repertoire of mutational signatures in human cancer. Nature. 2020;578:94–101. [PubMed: 32025018]

[20]. Argyris PP, Wilkinson PE, Jarvis MC, Magliocca KR, Patel MR, Vogel RI, et al. Endogenous APOBEC3B overexpression characterizes HPV-positive and HPV-negative oral epithelial dysplasias and head and neck cancers. Mod Pathol. 2021;34:280–90. [PubMed: 32632179]

[21]. Smith J, Tho LM, Xu N, Gillespie DA. The ATM-Chk2 and ATR-Chk1 pathways in DNA damage signaling and cancer. Adv Cancer Res. 2010;108:73–112. [PubMed: 21034966]

[22]. Ciccia A, Elledge SJ. The DNA damage response: making it safe to play with knives. Mol Cell. 2010;40:179–204. [PubMed: 20965415]

[23]. Lee JH, Paull TT. Activation and regulation of ATM kinase activity in response to DNA double-strand breaks. Oncogene. 2007;26:7741–8. [PubMed: 18066086]

[24]. Sancar A, Lindsey-Boltz LA, Unsal-Kaçmaz K, Linn S. Molecular mechanisms of mammalian DNA repair and the DNA damage checkpoints. Annu Rev Biochem. 2004;73:39–85. [PubMed: 15189136]

[25]. Norbury CJ, Zhivotovsky B. DNA damage-induced apoptosis. Oncogene. 2004;23:2797–808. [PubMed: 15077143]

[26]. Khammanivong A, Wang C, Sorenson BS, Ross KF, Herzberg MC. S100A8/A9 (calprotectin) negatively regulates G2/M cell cycle progression and growth of squamous cell carcinoma. PLoS One. 2013;8:e69395. [PubMed: 23874958]

[27]. Argyris PP, Slama ZM, Ross KF, Khammanivong A, Herzberg MC. Calprotectin and the Initiation and Progression of Head and Neck Cancer. J Dent Res. 2018;97:674–82. [PubMed: 29443623]

[28]. Silva EJ, Argyris PP, Zou X, Ross KF, Herzberg MC. S100A8/A9 regulates MMP-2 expression and invasion and migration by carcinoma cells. Int J Biochem Cell Biol. 2014;55:279–87. [PubMed: 25236491]

[29]. Bhattacharya S, Bunick CG, Chazin WJ. Target selectivity in EF-hand calcium binding proteins. Biochim Biophys Acta. 2004;1742:69–79. [PubMed: 15590057]

[30]. Champaiboon C, Sappington KJ, Guenther BD, Ross KF, Herzberg MC. Calprotectin S100A9 calcium-binding loops I and II are essential for keratinocyte resistance to bacterial invasion. J Biol Chem. 2009;284:7078–90. [PubMed: 19122197]

[31]. Khammanivong A, Sorenson BS, Ross KF, Dickerson EB, Hasina R, Lingen MW, et al. Involvement of calprotectin (S100A8/A9) in molecular pathways associated with HNSCC. Oncotarget. 2016;7:14029–47. [PubMed: 26883112]

[32]. Nisapakultorn K, Ross KF, Herzberg MC. Calprotectin expression in vitro by oral epithelial cells confers resistance to infection by Porphyromonas gingivalis. Infect Immun. 2001;69:4242–7. [PubMed: 11401960]

[33]. Zaia AA, Sappington KJ, Nisapakultorn K, Chazin WJ, Dietrich EA, Ross KF, et al. Subversion of antimicrobial calprotectin (S100A8/S100A9 complex) in the cytoplasm of TR146 epithelial cells after invasion by Listeria monocytogenes. Mucosal Immunol. 2009;2:43–53. [PubMed: 19079333]

[34]. Hsu K, Champaiboon C, Guenther BD, Sorenson BS, Khammanivong A, Ross KF, et al. ANTI-INFECTIVE PROTECTIVE PROPERTIES OF S100 CALGRANULINS. Antiinflamm Antiallergy Agents Med Chem. 2009;8:290–305. [PubMed: 20523765]

[35]. Argyris PP, Slama Z, Malz C, Koutlas IG, Pakzad B, Patel K, et al. Intracellular calprotectin (S100A8/A9) controls epithelial differentiation and caspase-mediated cleavage of EGFR in head and neck squamous cell carcinoma. Oral Oncol. 2019;95:1–10. [PubMed: 31345374]

[36]. Sorenson BS, Khammanivong A, Guenther BD, Ross KF, Herzberg MC. IL-1 receptor regulates S100A8/A9-dependent keratinocyte resistance to bacterial invasion. Mucosal Immunol. 2012;5:66–75. [PubMed: 22031183]

[37]. Tang XH, Knudsen B, Bemis D, Tickoo S, Gudas LJ. Oral cavity and esophageal carcinogenesis modeled in carcinogen-treated mice. Clin Cancer Res. 2004;10:301–13. [PubMed: 14734483]

[38]. Zhou G, Hasina R, Wroblewski K, Mankame TP, Doçi CL, Lingen MW. Dual inhibition of vascular endothelial growth factor receptor and epidermal growth factor receptor is an effective chemopreventive strategy in the mouse 4-NQO model of oral carcinogenesis. Cancer Prev Res (Phila). 2010;3:1493–502. [PubMed: 20978113]

[39]. Enari M, Sakahira H, Yokoyama H, Okawa K, Iwamatsu A, Nagata S. A caspase-activated DNase that degrades DNA during apoptosis, and its inhibitor ICAD. Nature. 1998;391:43–50. [PubMed: 9422506]

[40]. Nagata S Apoptotic DNA fragmentation. Exp Cell Res. 2000;256:12–8. [PubMed: 10739646]

[41]. Spoerri L, Oo ZY, Larsen JE, Haass NK, Gabrielli B, S. P. Cell Cycle Checkpoint and DNA Damage Response Defects as Anticancer Targets: From Molecular Mechanisms to Therapeutic Opportunities. In: Stress Response Pathways in Cancer. Wondrak Georg (Ed.) Springer. 2015. p. 29–49.

[42]. Bártová E, Legartová S, Dundr M, Suchánková J. A role of the 53BP1 protein in genome protection: structural and functional characteristics of 53BP1-dependent DNA repair. Aging (Albany NY). 2019;11:2488–511. [PubMed: 30996128]

[43]. Tarsounas M, Sung P. The antitumorigenic roles of BRCA1-BARD1 in DNA repair and replication. Nat Rev Mol Cell Biol. 2020;21:284–99. [PubMed: 32094664]

[44]. Oberdoerffer P, Miller KM. Histone H2A variants: Diversifying chromatin to ensure genome integrity. Semin Cell Dev Biol. 2022;S1084-9521(22)00078–7.

[45]. Imano N, Nishibuchi I, Kawabata E, Kinugasa Y, Shi L, Sakai C, et al. Evaluating Individual Radiosensitivity for the Prediction of Acute Toxicities of Chemoradiotherapy in Esophageal Cancer Patients. Radiat Res. 2021;195:244–52. [PubMed: 33400798]

[46]. Liskova V, Kajsik M, Chovancova B, Roller L, Krizanova O. Camptothecin, triptolide, and apoptosis inducer kit have differential effects on mitochondria in colorectal carcinoma cells. FEBS Open Bio. 2022;12:913–24.

[47]. Song R, Struhl K. S100A8/S100A9 cytokine acts as a transcriptional coactivator during breast cellular transformation. Sci Adv. 2021;7:eabe5357. [PubMed: 33523865]

[48]. Hanahan D, Weinberg RA. Hallmarks of cancer: the next generation. Cell. 2011;144:646–74. [PubMed: 21376230]

[49]. Solier S, Pommier Y. The apoptotic ring: a novel entity with phosphorylated histones H2AX and H2B and activated DNA damage response kinases. Cell Cycle. 2009;8:1853–9. [PubMed: 19448405]

[50]. Gionchiglia N, Granato A, Merighi A, Lossi L. Association of Caspase 3 Activation and H2AX γ Phosphorylation in the Aging Brain: Studies on Untreated and Irradiated Mice. Biomedicines. 2021;9:1166. [PubMed: 34572352]

[51]. Yu H, Harrison FE, Xia F. Altered DNA repair; an early pathogenic pathway in Alzheimer's disease and obesity. Sci Rep. 2018;8:5600. [PubMed: 29618789]

[52]. Ghavami S, Kerkhoff C, Los M, Hashemi M, Sorg C, Karami-Tehrani F. Mechanism of apoptosis induced by S100A8/A9 in colon cancer cell lines: the role of ROS and the effect of metal ions. J Leukoc Biol. 2004;76:169–75. [PubMed: 15075348]

[53]. Sattari M, Pazhang Y, Imani M. Calprotectin induces cell death in human prostate cancer cell (LNCaP) through survivin protein alteration. Cell Biol Int. 2014;38:1311–20. [PubMed: 24942387]

[54]. Zhu Y, Zhang F, Zhang S, Deng W, Fan H, Wang H, et al. Regulatory mechanism and functional analysis of S100A9 in acute promyelocytic leukemia cells. Front Med. 2017;11:87–96. [PubMed: 28063140]

[55]. Qin F, Song Y, Li Z, Zhao L, Zhang Y, Geng L. S100A8/A9 induces apoptosis and inhibits metastasis of CasKi human cervical cancer cells. Pathol Oncol Res. 2010;16:353–60. [PubMed: 19957061]

[56]. Vogl T, Ludwig S, Goebeler M, Strey A, Thorey IS, Reichelt R, et al. MRP8 and MRP14 control microtubule reorganization during transendothelial migration of phagocytes. Blood. 2004;104:4260–8. [PubMed: 15331440]

[57]. Markowitz J, Carson WE. Review of S100A9 biology and its role in cancer. Biochim Biophys Acta. 2013;1835:100–9. [PubMed: 23123827]

[58]. Schenten V, Plançon S, Jung N, Hann J, Bueb JL, Bréchard S, et al. Secretion of the Phosphorylated Form of S100A9 from Neutrophils Is Essential for the Proinflammatory Functions of Extracellular S100A8/A9. Front Immunol. 2018;9:447. [PubMed: 29593718]

[59]. Davis AJ, Chen DJ. DNA double strand break repair via non-homologous end-joining. Transl Cancer Res. 2013;2:130–43. [PubMed: 24000320]

Major highlights of our cell line and animal tissue studies include:

1. S100A8/A9 potentiates DNA damage responses and nuclear localization of 53BP1 and γH2AX after treatment with genotoxic agents, i.e., camptothecin and X-irradiation.
2. Calprotectin promotes apoptotic DNA fragmentation and cell death following X-irradiation and cisplatin treatment in head and squamous cell carcinoma cell lines.
3. Calprotectin expression is associated with increased 53BP1 expression levels in carcinogen-induced mouse oral epithelial dysplastic and carcinomatous lesions.

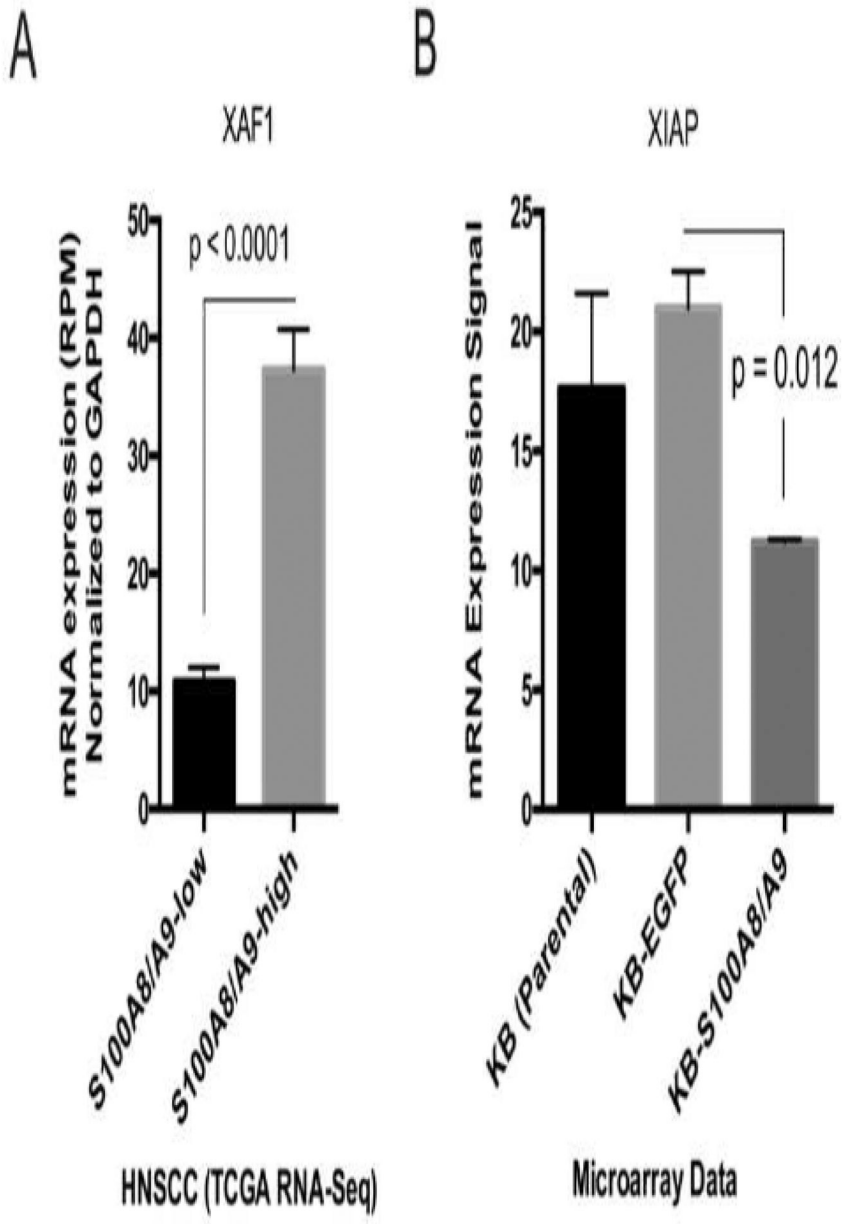

Figure 1:

(A) S100A8/A9-high human HNSCCs (n=104) significantly upregulated the mRNA levels of the apoptosis-promoting XIAP-associated factor 1 (*XAF1*) when compared to S100A8/A9-low tumors (n=89) based on TCGA analysis (mean ± SEM, $p < 0.0001$, two-tailed Student's t-test with equal variance). **(B)** KB carcinoma cells stably expressing S100A8/A9 significantly downregulated the anticaspase X-linked inhibitor of apoptosis (*XIAP*) *in vitro* compared to S100A8/A9-negative KB-EGFP cells (n = 2, mean ± SD, $p = 0.012$, one-way ANOVA test).

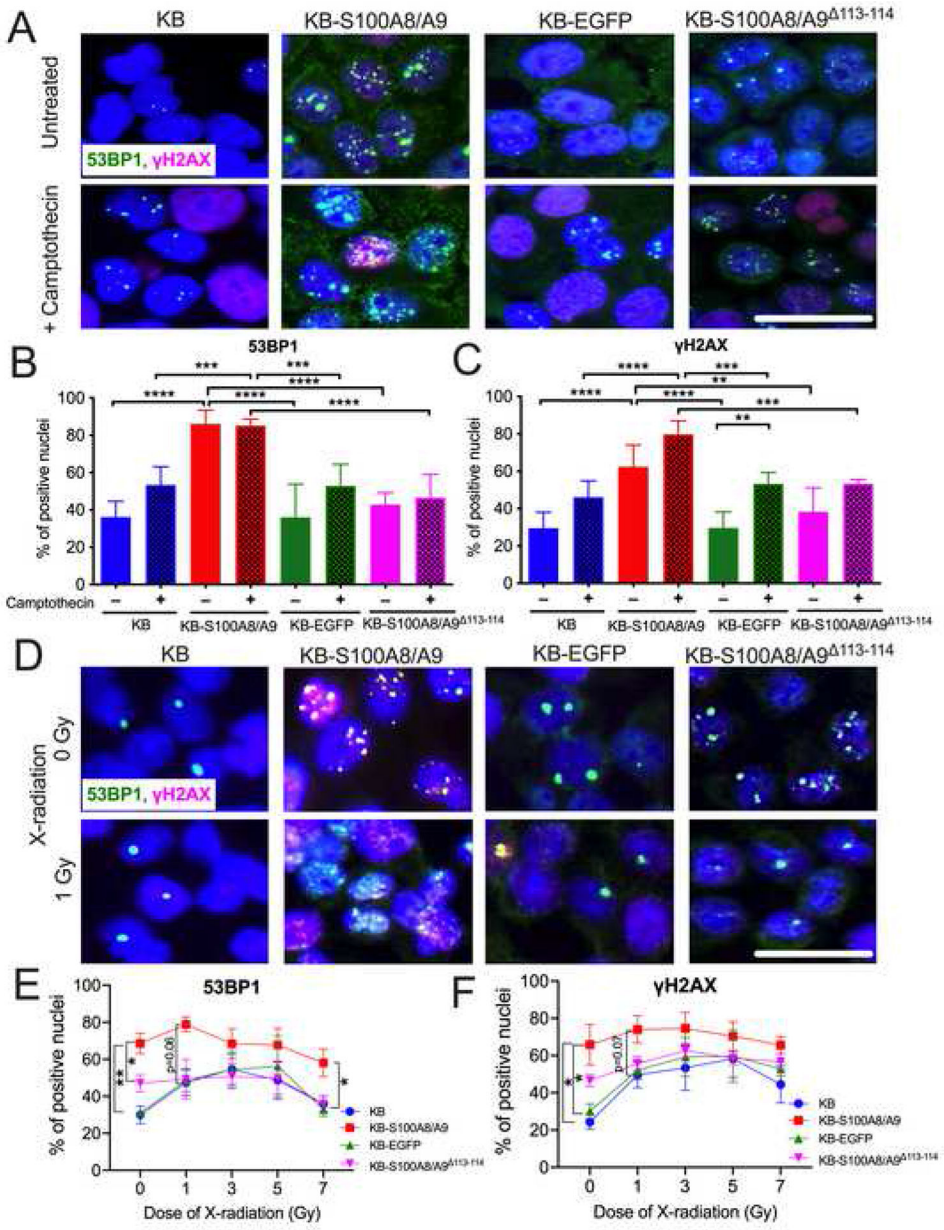

Figure 2:

(A) Immunofluorescence microscopy showing DDR-related markers 53BP1 (green) and γH2AX (purple) in calprotectin-negative KB and KB-EGFP cells, and KB cells expressing either wild-type human calprotectin (KB-S100A8/A9) or a truncated non-phosphorylatable clone (KB-S100A8/A9$^{\Delta 113–114}$) after camptothecin treatment (scale bar = 50 μm). **(B)** Quantification of the percentages of 53BP1 positive nuclei before and after camptothecin treatment. Ectopic expression of wild-type human calprotectin in KB cancer cells yields increased 53BP1 expression compared to calprotectin-negative KB, KB-EGFP, and the non-phosphorylatable KB-S100A8/A9$^{\Delta 113–114}$ cells. Statistically significant differences are shown. **(C)** Quantification of the percentages of γH2AX positive nuclei. Intracellular calprotectin expression potentiates nuclear recruitment of γH2AX in addition to 53BP1 after

camptothecin-induced DNA damage. Statistically significant differences are shown (for both B and C, N = 5, mean ± SD, ** $p < 0.01$, *** $p < 0.001$, **** $p < 0.0001$ one-way ANOVA test). **(D)** 53BP1 (green) and γH2AX (purple) visualized at 0 and 1 Gy of X-irradiation using immunofluorescence microscopy (scale bar = 50 μm). **(E, F)** Quantification of the percentages of 53BP1 and γH2AX positive nuclei from immunofluorescence experiments in (D). Phosphorylatable S100A8/A9 overexpression in KB carcinoma cells facilitated and promoted recruitment of DDR-related proteins in the nucleus after X-irradiation. Statistically significant differences are shown (N = 3, mean ± SEM, * $p < 0.05$, ** $p < 0.01$, one-way ANOVA test).

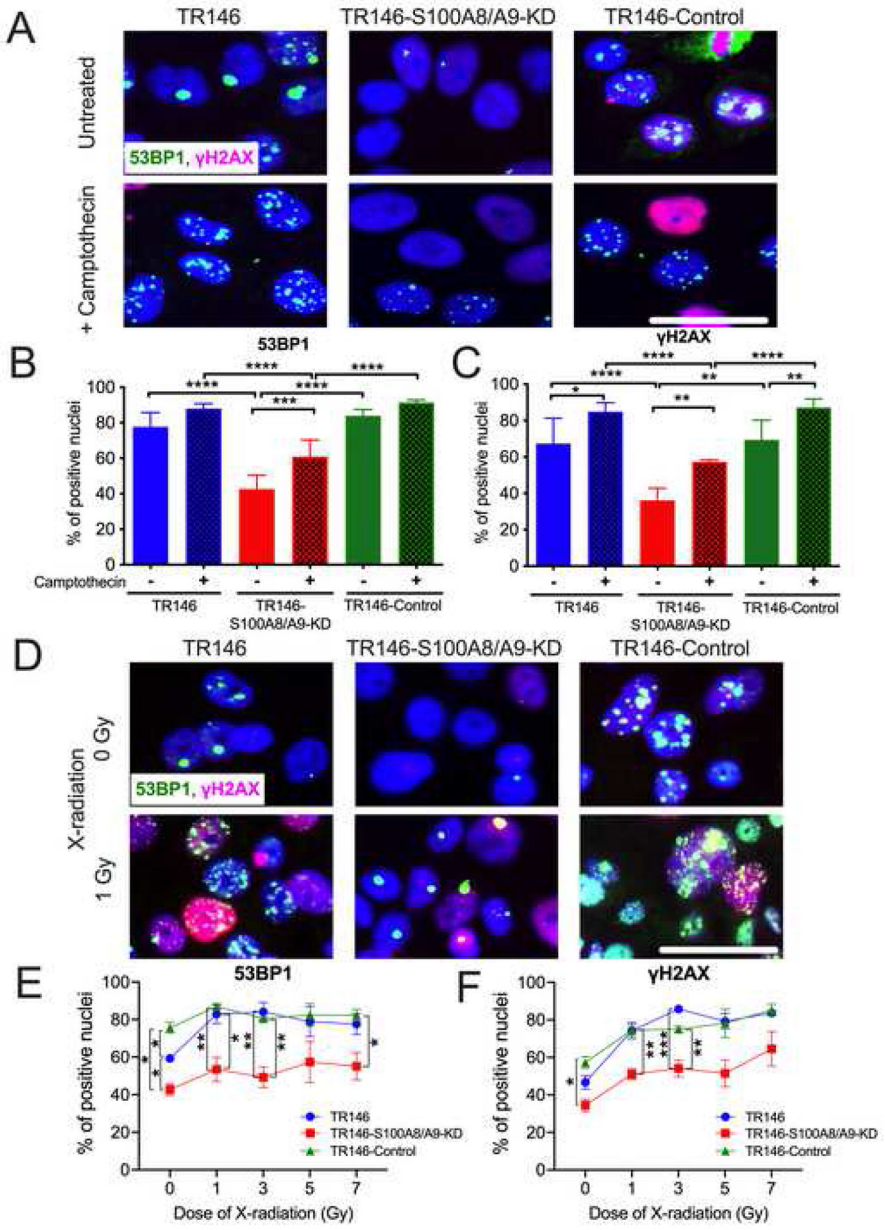

Figure 3:

(A) Immunofluorescence microscopy showing 53BP1 (green) and γH2AX (purple) nuclear puncta in calprotectin-positive TR146 and TR146-control carcinoma cells, and TR146 cells with silenced calprotectin expression (TR146-S100A8/A9-KD), following camptothecin treatment (scale bar=50μm). **(B, C)** Silencing S100A8/A9 in TR146 cells diminished DDR and nuclear recruitment of 53BP1 and γH2AX; quantification of the percentages of 53BP1 and γH2AX positive nuclei from immunofluorescence experiments shown in (A). Statistically significant differences are shown (N = 6, mean ± SD, * $p < 0.05$, ** $p < 0.01$, *** $p < 0.001$, **** $p < 0.0001$ one-way ANOVA test). **(D)** Foci of 53BP1 and γH2AX visualized at 0 and 1 Gy of X-irradiation using immunofluorescence microscopy (scale bar = 50 μm). **(E, F)** Silencing S100A8/A9 in TR146 cells impaired DDR after exposure

to increasing doses of X-irradiation; percentages of 53BP1 and γH2AX positive nuclei quantified from immunofluorescence experiments in (D). Statistically significant differences are shown (N = 3, mean ± SEM, * $p < 0.05$, ** $p < 0.01$, *** $p < 0.001$ one-way ANOVA test).

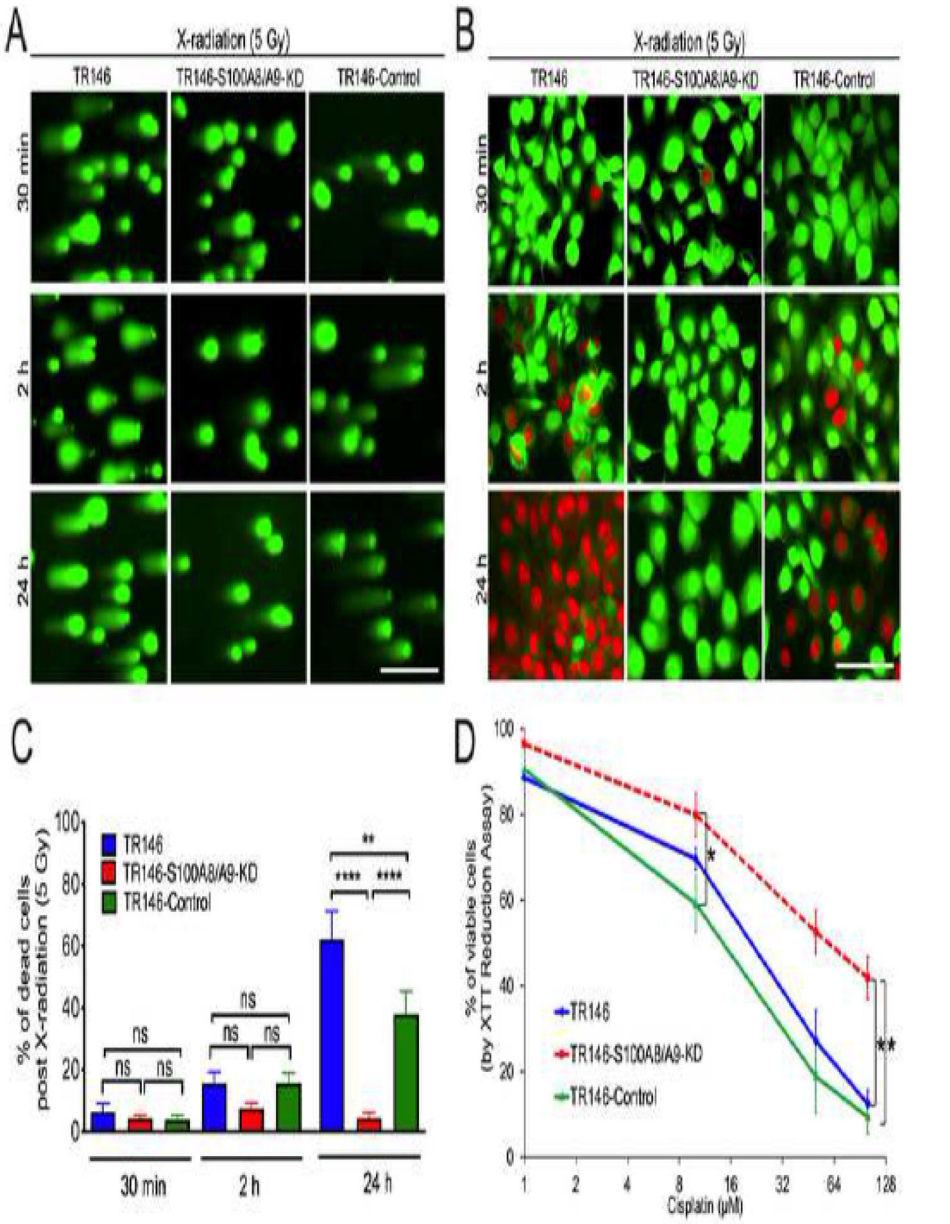

Figure 4:

(A) Single cell gel electrophoresis of TR146, TR146-S100A8/A9-KD, and TR146-control cells after exposure to 5 Gy of X-irradiation. S100A8/A9-producing TR146 and TR146-control cells appeared more sensitive to X-irradiation and showed greater nuclear fragmentation and comet tail formation than calprotectin-silenced (TR146-S100A8/A9-KD) cells (scale bar = 100 μm). **(B)** Live/dead assay following exposure to a single dose of 5 Gy of X-radiation. S100A8/A9-expressing TR146 and TR146-control cells showed a significantly higher percentage of apoptotic cells (red) than TR146-S100A8/A9-KD carcinoma cells which appeared mostly viable (green) 24 h after X-irradiation (scale bar = 60 μm). **(C)** Quantification of the immunofluorescence experiments shown in (B). Statistically significant differences are shown (N = 3, mean ± SEM, ** $p < 0.01$, **** p

< 0.0001, one-way ANOVA test). **(D)** TR146, TR146-S100A8/A9-KD and TR146-control cell viability assay after incubation for 24 h with increasing doses (1, 10, 50 and 100 μM) of cisplatin. Silencing of S100A8/A9 in this oral SCC cell line increases their resistance to cisplatin treatment. Statistically significant differences are shown (N = 5, mean ± SEM, * p < 0.05, one-way ANOVA test).

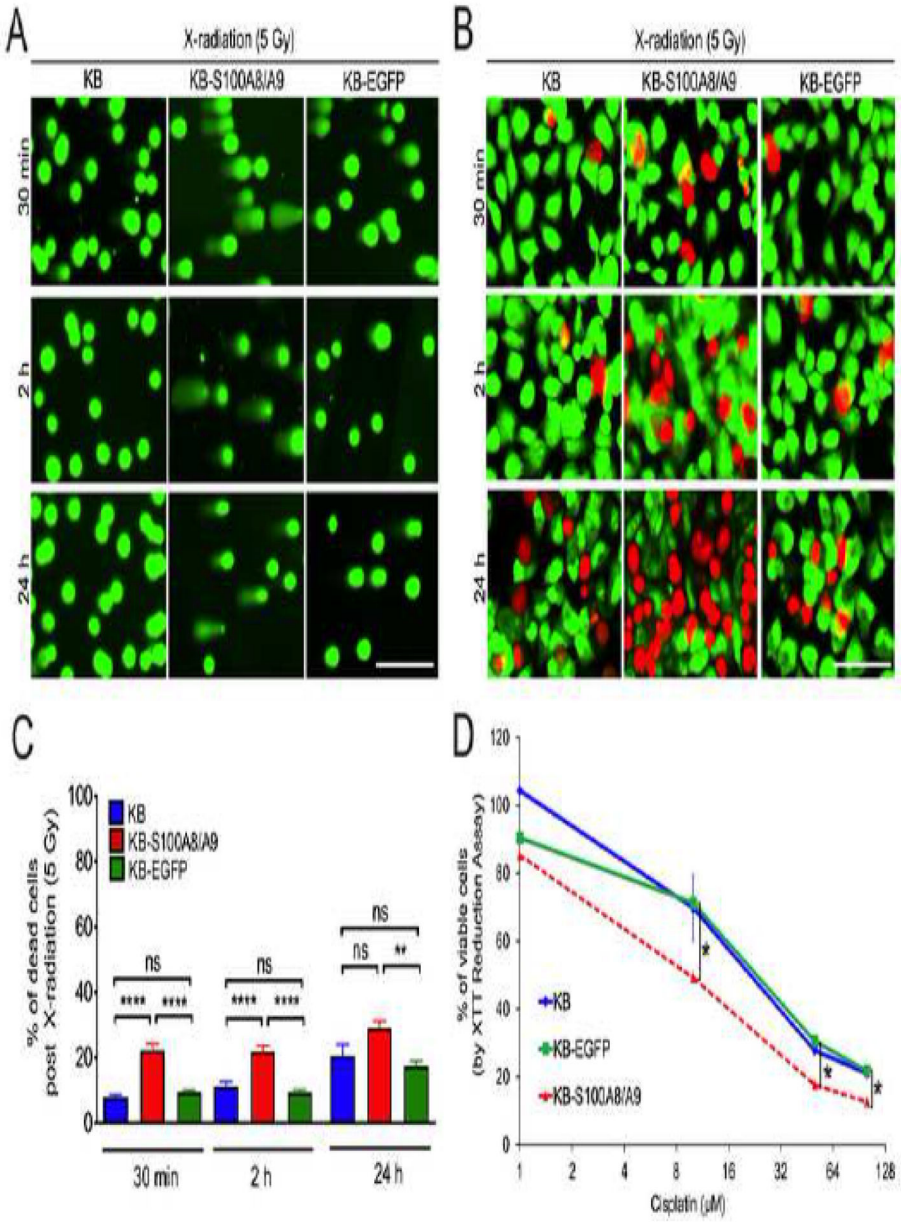

Figure 5:

(A) Single cell gel electrophoresis of KB, KB-S100A8/A9, and KB-EGFP cells after exposure to 5 Gy of X-irradiation. KB-S100A8/A9 cells showed greater comet tail formation than calprotectin-negative KB and KB-EGFP cells (scale bar = 100 μm). **(B)** Live/dead assay following exposure to a single dose of 5 Gy of X-radiation. KB-S100A8/A9 cells showed significantly higher proportions of dead cells (red) at 30 min, 2 h and 24 h after X-irradiation than KB and KB-EGFP cells which appeared radiotherapy-resistant and mostly viable (green, scale bar = 60 μm). **(C)** Quantification of the immunofluorescence experiments shown in (B). Statistically significant differences are shown (N = 3, mean ± SEM, ** $p < 0.01$, **** $p < 0.0001$, one-way ANOVA test). **(D)** KB, KB-S100A8/A9 and KB-EGFP cell viability assay after incubation for 24 h with cisplatin (1, 10, 50 and 100 μM). Calprotectin

overexpression conferred sensitivity to chemotherapy in these carcinoma cells. Statistically significant differences are shown (N = 2, mean ± SEM, * $p < 0.05$, one-way ANOVA test).

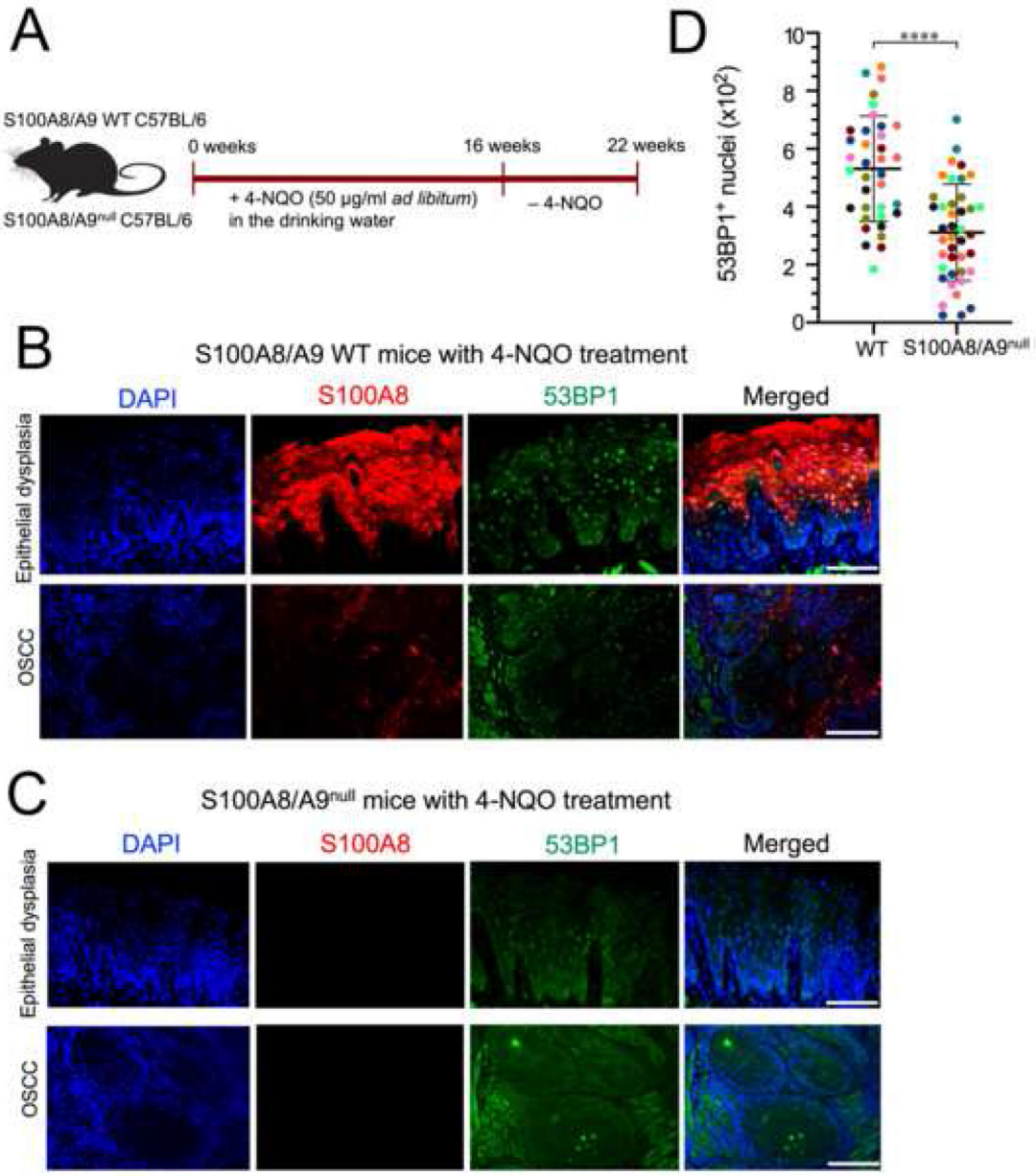

Figure 6:

(A) Experimental design of 4-NQO-induced oral carcinogenesis in S100A8/A9 wild-type (WT) and S100A8/A9^{null} C57BL/6j mice. **(B)** Representative photomicrographs of 4-NQO-induced lingual epithelial dysplasias and OSCC in S100A8/A9 WT mice stained for 53BP1 (green) and S100A8 (red). The calprotectin-subunit S100A8 serves as surrogate marker for the calprotectin complex. 53BP1 nuclear puncta were prominent in the dysplastic oral epithelium of calprotectin-expressing mice, but were less apparent in SCC tumors, which featured decreased expression of S100A8 (scale bar = 200 µm). **(C)** Representative photomicrographs of 4-NQO-induced oral lesions in S100A8/A9^{null} mice stained for S100A8 and 53BP1. Calprotectin-negative mice showed rare 53BP1 expression in tongue dysplastic and carcinomatous lesions (scale bar = 200 µm). **(D)** Quantification of 53BP1-

positive nuclei from oral epithelial dysplasias and OSCC is shown in (B) and (C). 53BP1 expression in 4-NQO-induced oral lesions was significantly higher in WT calprotectin-expressing mice than in calprotectin-negative mutants. Same color indicates lesions from the same mouse (N = 7 animals/group, total number of lesions = 36 for WT and 41 for S100A8/A9^{null} mice, mean ± SD, **** $p < 0.0001$, unpaired t-test).

Table 1.

Caspase family members that appear upregulated in S100A8/A9-high head and neck squamous cell carcinoma (HNSCC) specimens compared to S100A8/A9-low tumors.

Apoptosis-related genes[a]	Fold-Change S100A8/A9-High vs -Low HNSCC	p-value[b]
CASP1	2.34	**6.18E-10**
CASP10	3.78	**3.61E-17**
CASP12	1.56	0.106
CASP14	9.54	**0.0395**
CASP2	1.06	0.5663
CASP3	1.48	**0.0005**
CASP4	3.54	**2.60E-20**
CASP5	2.76	**3.54E-05**
CASP6	1.16	0.099
CASP7	1.87	**1.39E-08**
CASP8	2.02	**9.00E-09**
CASP9	1.50	**0.0003**

[a] Publicly available RNAseq data mined from The Cancer Genome Atlas (TCGA).

[b] Bolded p-values indicate statistically significant differences using a two-tailed Student's t-test with equal variance.